https://doi.org/10.5194/egusphere-2026-6659
Preprint. Discussion started: 22 November 2026
© Author(s) 2026. CC BY 4.0 License.

Evaluating EarthCARE ATLID aerosol optical products under varying dust loads: Insights from ground-based observations in the Taklimakan Desert

Yabin Wei[1,2,3,4,5], Yu Wang[1,2,3,4,5], Ali Mamtimin[1,2,3,4,5],Meiqi Song[1,2,3,4,5],Jiacheng Gao[1,2,3,4,5], Yakupujiang Abuduaini[6], Cong Wen[1,2,3,4,5],Qing Gong[5]

[1] Institute of Desert Meteorology, China Meteorological Administration, Urumqi 830002, China
[2] National Observation and Research Station of Desert Meteorology, Taklimakan Desert of Xinjiang, Urumqi 830002, China
[3] Taklimakan Desert Meteorology Field Experiment Station of China Meteorological Administration, Urumqi 830002, China
[4] Xinjiang Key Laboratory of Desert Meteorology and Sandstorm, Urumqi 830002, China
[5] Tazhong National Climate Observatory, Qiemo 841999, China
[6] School of Remote Sensing and Geomatics Engineering, Nanjing University of Information Science and Technology, Nanjing, 210044, China

Correspondence to: Ali Mamtimin (ali@idm.cn)

Abstract. The Atmospheric Lidar (ATLID) aboard the EarthCARE satellite provides new observational capabilities for investigating the vertical structure and optical properties of dust aerosols; however, its product performance in regions affected by heavy dust loading requires validation against ground-based observations. In this study, the extinction coefficient, backscatter coefficient, particle linear depolarization ratio, and lidar ratio from the ATLID L2A A-EBD product were evaluated using 17 satellite–ground collocation cases at Aksu, Tazhong, and Minfeng during spring and summer 2025. The assessment integrated analyses of representative dust events, multi-site statistics, vertical bias distributions, and nighttime Raman lidar observations. The results indicate that ATLID generally captures the main altitude ranges and vertical structures of dust layers, although quantitative agreement varies among parameters and stations. Across the three stations, extinction correlation coefficients ranged from 0.69 to 0.88, with mean bias percentages (MBPs) of 17.6%–48.0%, while backscatter correlation coefficients ranged from 0.36 to 0.87, with MBPs of 72.3%–159.5%. Agreement in the depolarization ratio was relatively weaker, with correlation coefficients from −0.52 to 0.09, mean biases of 0.148–0.214, and MBPs of 95.1%–300.3%. Positive extinction and backscatter biases were mainly concentrated within aerosol layers at lower and middle altitudes, whereas positive depolarization ratio biases were distributed over a broader range of altitudes. A single nighttime Raman lidar comparison showed closer agreement in the overall backscatter structure than in extinction, depolarization ratio, and lidar ratio, with some localized enhancements being less apparent in the ATLID profiles. Within the available samples, biases showed no clear systematic relationship with either horizontal distance or ground-based aerosol optical depth (AOD). These findings support the capability of ATLID to characterize the main vertical structures of dust layers, while also indicating that parameter-

https://doi.org/10.5194/egusphere-2026-6659
Preprint. Discussion started: 22 November 2026
© Author(s) 2026. CC BY 4.0 License.

specific quality screening, uncertainty assessment, and further independent validation are still required to support quantitative applications of its optical products.

1 Introduction

Dust aerosols play an important role in the Earth system by influencing the radiative budget, cloud microphysical processes, and biogeochemical cycles. Dust particles scatter and absorb radiation and modify cloud macrophysical and microphysical properties, thereby affecting regional climate (Huang et al., 2006; Huang et al., 2014; Kok et al., 2023). Atmospheric heating caused by dust absorption can also influence local thermal structure and boundary-layer evolution (Zhou et al., 2022). Furthermore, dust particles can act as ice-nucleating particles and, under suitable conditions, cloud condensation nuclei, thereby affecting cloud and precipitation processes (Chen et al., 2026; Zhou et al., 2025). Understanding these effects requires information on both dust loading and its vertical distribution relative to clouds. However, dust emission, uplift, transport, and boundary-layer mixing produce substantial spatial heterogeneity and vertical variability. Passive remote sensing provides extensive observations of column-integrated aerosol properties, and some techniques can also estimate dust-layer height, but constraints on detailed vertical structure remain limited (Kylling et al., 2018; Remer et al., 2024). Combining lidar and passive observations helps characterize both column properties and vertical distributions, providing valuable reference information for evaluating satellite products and atmospheric models (Benavent-Oltra et al., 2021).

Spaceborne lidar provides vertically resolved observations of aerosols and clouds across broad geographical regions and is an important tool for investigating aerosol layering and aerosol–cloud vertical relationships (Hong and Di Girolamo, 2022; Winker et al., 2009). Since its launch in 2006, the Cloud–Aerosol Lidar and Infrared Pathfinder Satellite Observations (CALIPSO) mission, carrying the Cloud-Aerosol Lidar with Orthogonal Polarization (CALIOP), has substantially advanced understanding of aerosol vertical distributions and transport (Winker et al., 2010). CALIOP observations have been widely used for aerosol extinction retrievals, aerosol classification, and dust climatology studies (Omar et al., 2009; Song et al., 2021; Young and Vaughan, 2009). However, as an elastic-backscatter lidar, CALIOP generally relies on prescribed, aerosol-type-dependent lidar ratios to retrieve aerosol extinction. For example, the Version 4 algorithm assigns mineral dust a lidar ratio of 44 ± 9 sr at 532 nm (Kim et al., 2018). Errors in aerosol classification and differences between prescribed and actual lidar ratios can affect the retrievals, highlighting the need for additional independent observational constraints on aerosol optical properties.

Launched in 2024, the Earth Cloud, Aerosol and Radiation Explorer (EarthCARE) mission provides new opportunities for investigating aerosol vertical structure. Its Atmospheric LIDar (ATLID) is a polarization-sensitive high-spectral-resolution lidar operating at 355 nm that separates molecular and particulate backscatter signals, providing additional constraints for extinction and backscatter retrievals (Wehr et al., 2023). Nevertheless, signal processing and retrievals under low signal-to-noise conditions still require appropriate smoothing and parameter constraints. The ATLID FeatureMask (A-FM) product provides feature-detection information and guides subsequent smoothing procedures (Van Zadelhoff et al., 2023). The

https://doi.org/10.5194/egusphere-2026-6659
Preprint. Discussion started: 22 November 2026
© Author(s) 2026. CC BY 4.0 License.

extinction, backscatter, and depolarization product (A-EBD) uses an optimal-estimation approach informed by prior information from A-AER and assumes a constant lidar ratio within each identified layer (Donovan et al., 2024). Independent validation therefore remains necessary to assess how effectively these products represent aerosol structure and optical properties. Recent PollyNET validation demonstrated that A-EBD reproduces aerosol vertical structure well across several environments, while quantitative performance varies among parameters, with substantial aerosol depolarization-ratio discrepancies in processing baselines BA and BB (Baars et al., 2026). These findings highlight the need for further evaluation across different dust-loading and layering conditions in major dust source regions.

The Taklamakan Desert is an important Asian dust source characterized by frequent dust activity and substantial spatiotemporal variability (Jin et al., 2024). Influenced by the surrounding topography and atmospheric circulation, dust emitted from this region can reach the free troposphere and undergo long-range transport across East Asia and the Pacific (Yumimoto et al., 2009). Dust deposition can also reduce snow albedo in the surrounding mountains, affecting the regional radiative budget (Xing et al., 2024). The variable dust loading and complex vertical structure make this region particularly relevant for evaluating spaceborne lidar products. At the same time, spatial heterogeneity complicates comparisons between satellite profiles and observations at fixed ground stations. The representativeness of ground-based observations depends not only on collocation distance but also on the spatiotemporal homogeneity of the target (Floutsi et al., 2026). Coordinated observations from multiple stations can therefore provide complementary spatial information to assess satellite performance and interpret differences under varying local conditions.

In this study, ground-based lidar observations at Aksu, Minfeng, and Tazhong are used to evaluate the EarthCARE/ATLID L2A A-EBD product during dust events over the Taklamakan Desert. For each comparison, the ATLID profile closest to the station is paired with the ground-based profile nearest in time to its acquisition. Case studies and statistical comparisons assess the representation of major dust layers and the agreement and biases in particle extinction coefficient, backscatter coefficient, and particle linear depolarization ratio. The Minfeng–Tazhong observations provide spatial context for interpreting satellite–ground differences, while a Raman lidar case provides an additional reference for evaluating extinction, backscatter, and lidar ratio. We further examine how mean biases vary with horizontal separation and aerosol loading, represented by ground-based aerosol optical depth (AOD), to assess their relationships with satellite–ground agreement. These analyses provide a regional observational assessment of A-EBD and help clarify its capabilities and limitations for investigating dust vertical structure.

2 Instrumentation and methods

2.1 Study site and ground-based lidar observations

Ground-based lidar observations at Tazhong, Aksu, and Minfeng were used to evaluate EarthCARE/ATLID aerosol optical products during dust events over the Taklamakan Desert. These sites represent the desert interior, an oasis along the northwestern desert margin, and the southern desert margin, respectively. Their locations and elevations are listed in Table 1. Together, the three sites provide complementary observations across different geographical settings and dust-loading

https://doi.org/10.5194/egusphere-2026-6659
Preprint. Discussion started: 22 November 2026
© Author(s) 2026. CC BY 4.0 License.

conditions, allowing an assessment of both site-specific performance and spatial variability in satellite–ground agreement. Ground-based profiles of particle extinction coefficient, backscatter coefficient, and particle linear depolarization ratio at 355 nm were used as reference observations for the corresponding ATLID A-EBD products.

Table 1 Locations and elevations of the ground-based lidar sites used to evaluate EarthCARE ATLID aerosol optical products during selected dust cases.

Name	Latitude(°N)	Longitude(°E)	Altitude(m asl)
Tazhong	38.9675	83.6597	1100.6
Aksu	41.1186	80.3819	1107.1
Minfeng	37.0678	82.6908	1408.9

Tazhong is equipped with a GBQ L-03 three-wavelength, eight-channel Raman polarization lidar manufactured by Hefei Zhongke Guangbo Quantum Technology Co., Ltd. Aksu and Minfeng operate YLJ1 Raman–Mie aerosol lidars manufactured by Wuxi Zhongke Optoelectronics Technology Co., Ltd. All three systems emit laser pulses at 355, 532, and 1064 nm. The Tazhong data used in this study have temporal and vertical resolutions of 10 min and 7.5 m, respectively, whereas the corresponding resolutions at Aksu and Minfeng are 5 min and 15 m. The instrument models and data resolutions are summarized in Table 2.

Table 2 Ground-based lidar systems and data resolutions used in this study.

Site	Model	Emitted wavelengths (nm)	Temporal resolution (min)	Vertical resolution (m)
Tazhong	GBQ L-03	355, 532, 1064	10	7.5
Aksu	YLJ1	355, 532, 1064	5	15
Minfeng	YLJ1	355, 532, 1064	5	15

The ground-based extinction and backscatter profiles at 355 nm used in the main satellite–ground comparisons were retrieved using the Fernald method (Fernald, 1984). This method requires a prescribed aerosol lidar ratio and a boundary condition at a reference altitude; consequently, the retrieved extinction and backscatter coefficients are coupled through the assumed lidar ratio. Nighttime Raman observations at Tazhong were analysed separately to retrieve extinction and backscatter without prescribing an aerosol lidar ratio (Ansmann et al., 1992). The ratio of these Raman-derived quantities was then used to obtain the lidar ratio at 355 nm, providing an additional reference for the case-based evaluation of ATLID optical properties. Continuous lidar observations were used to characterize the temporal evolution of aerosol vertical structure around each satellite overpass. For quantitative comparisons, the ground-based profile nearest in time to the acquisition of the selected ATLID profile was used, subject to the specified temporal matching criterion. Following quality control, the matched profiles were resampled onto a common altitude grid with 100 m spacing to facilitate comparisons at corresponding heights.

2.2 EarthCARE ATLID aerosol optical products

The Atmospheric Lidar (ATLID) aboard EarthCARE, a joint ESA–JAXA mission, is a polarisation-sensitive high-spectral-resolution lidar operating at 355 nm (Wehr et al., 2023). Its molecular, particulate, and cross-polarisation measurements

https://doi.org/10.5194/egusphere-2026-6659
Preprint. Discussion started: 22 November 2026
© Author(s) 2026. CC BY 4.0 License.

provide information on the vertical structure and optical properties of aerosols and clouds. In the ESA processing chain, the ATLID profile processor (A-PRO) generates the A-AER and A-EBD products. A-AER provides large-scale aerosol optical information, while A-EBD uses an optimal-estimation framework informed by A-AER to retrieve optical profiles (Donovan et al., 2024). This study uses the low-resolution version of the Level 2A A-EBD product (ATL_EBD_2A), including particle extinction coefficient, backscatter coefficient, particle linear depolarisation ratio, and lidar ratio at 355 nm. The analysis covers March–August 2025, and Baseline BA products were used consistently across all selected overpasses. The profiles are provided on the Joint Standard Grid, with approximately 1 km along-track sampling and 100 m vertical sampling in the troposphere (Eisinger et al., 2024). However, the low-resolution aerosol fields incorporate horizontal smoothing over approximately 100 km; therefore, the output grid spacing does not represent their effective horizontal resolution (Baars et al., 2026). This smoothing reduces random noise but may suppress local variability and introduce spatial dependence between neighbouring profiles. Consequently, even the satellite profile closest to a ground station represents aerosol conditions over a broader horizontal extent than its nominal grid spacing. Observation time, geolocation, height, classification, and quality information were also extracted for collocation and screening. Extinction and backscatter coefficients were converted to km^{-1} and $km^{-1}\ sr^{-1}$, respectively; particle linear depolarisation ratios are dimensionless, and lidar ratios are expressed in steradians. The quality-control, collocation, and profile-harmonisation procedures are described in Sect. 2.3.

2.3 Collocation and evaluation methods

EarthCARE overpasses with ground tracks passing within 100 km of Aksu, Tazhong, or Minfeng were selected. For each station, the single ATLID L2A A-EBD profile closest to the station was extracted, and its acquisition time was defined as the station-specific reference overpass time. The ground-based lidar profile nearest in time to this reference was then selected for comparison. No additional spatial or temporal averaging of neighbouring profiles was performed. All times were converted to Beijing time (BJT, UTC+8). Each station–overpass pair constituted one comparison case. Pairs involving multiple stations during the same overpass were retained but were not considered fully independent events. Dust cases were identified using meteorological station weather phenomenon records. The record nearest in time to the reference overpass time was selected, and cases with recorded codes of 6, 7, or 33 were classified as dust cases. Ground-based lidar heights above ground level were converted to altitudes above mean sea level by adding the station elevation. Satellite and ground-based profiles were then mapped onto a common altitude grid from 100 to 10,000 m at 100 m intervals using bin averaging. Valid observations within each altitude bin were averaged separately for the two datasets, and bins without valid observations were treated as missing. Comparisons were restricted to altitude bins with valid observations from both instruments. For the scatter plots, a mask derived from the ground-based extinction profile was used to exclude background-dominated samples. For each optical parameter, the relative bias at altitude bin i was calculated as Eq.(1):

$$bias_i = \frac{X_{SAT,i} - X_{GND,i}}{X_{GND,i}} \times 100\% \quad (1)$$

https://doi.org/10.5194/egusphere-2026-6659
Preprint. Discussion started: 22 November 2026
© Author(s) 2026. CC BY 4.0 License.

where $X_{SAT,i}$ and $X_{GND,i}$ denote the satellite and ground-based values, respectively. The mean relative bias for each comparison case was calculated as Eq.(2):

$$\overline{bias} = \frac{1}{N}\sum_{i=1}^{N} bias_i \quad (2)$$

where N is the number of valid paired altitude bins included in the calculation. Missing values and bins with zero ground-based values were excluded. Positive and negative biases indicate satellite values higher and lower than the ground-based values, respectively.

Ground-based aerosol optical depth (AOD) at 355 nm, calculated as described in Eq. (3), was used to characterize aerosol loading during the dust cases.

$$AOD_{GND,355} = \int_{z_{min}}^{z_{max}} \alpha_{GND,355} dz \quad (3)$$

where z_{max} and z_{min} are the lower and upper integration limits. Height is expressed in kilometres when extinction is given in km^{-1}. Case-specific mean relative biases were examined against horizontal distance and ground-based AOD to assess their relationships with spatial separation and aerosol loading.

3 Result

3.1 Overview and representativeness of collocated observations

Following screening based on meteorological station weather phenomenon records and cloud-cover conditions, 17 EarthCARE–ground-based lidar overpass collocation cases were retained: five at Aksu, six at Tazhong, and six at Minfeng. The three stations are located on the northern margin of the Tarim Basin, in the interior of the Taklimakan Desert, and on its southern margin, respectively, providing reference observations for satellite–ground dust validation across different geographical settings (Fig. 2a). All selected tracks passed within 100 km of the corresponding station. Some overpasses met the distance criterion for both Tazhong and Minfeng, enabling coordinated validation at two stations. The cases span spring and summer 2025, with ground-based lidar-derived AOD ranging from approximately 0.2 to 3.7, indicating a broad range of optical loading among the selected dust cases (Fig. 2b). Minfeng exhibited substantial AOD variability and the highest value among the observations, whereas the Aksu and Tazhong cases mainly occupied relatively lower AOD ranges. Both daytime and nighttime observations were included, although their temporal distributions and proportions differed among stations. Overpass distances ranged from approximately 8 to 93 km and varied considerably among stations and cases (Fig. 2c). Consequently, both optical loading and spatial matching conditions need to be considered when interpreting satellite–ground differences. Each station–overpass match constituted one comparison case, while matches involving multiple stations during the same overpass were not considered fully independent events.

https://doi.org/10.5194/egusphere-2026-6659
Preprint. Discussion started: 22 November 2026
© Author(s) 2026. CC BY 4.0 License.

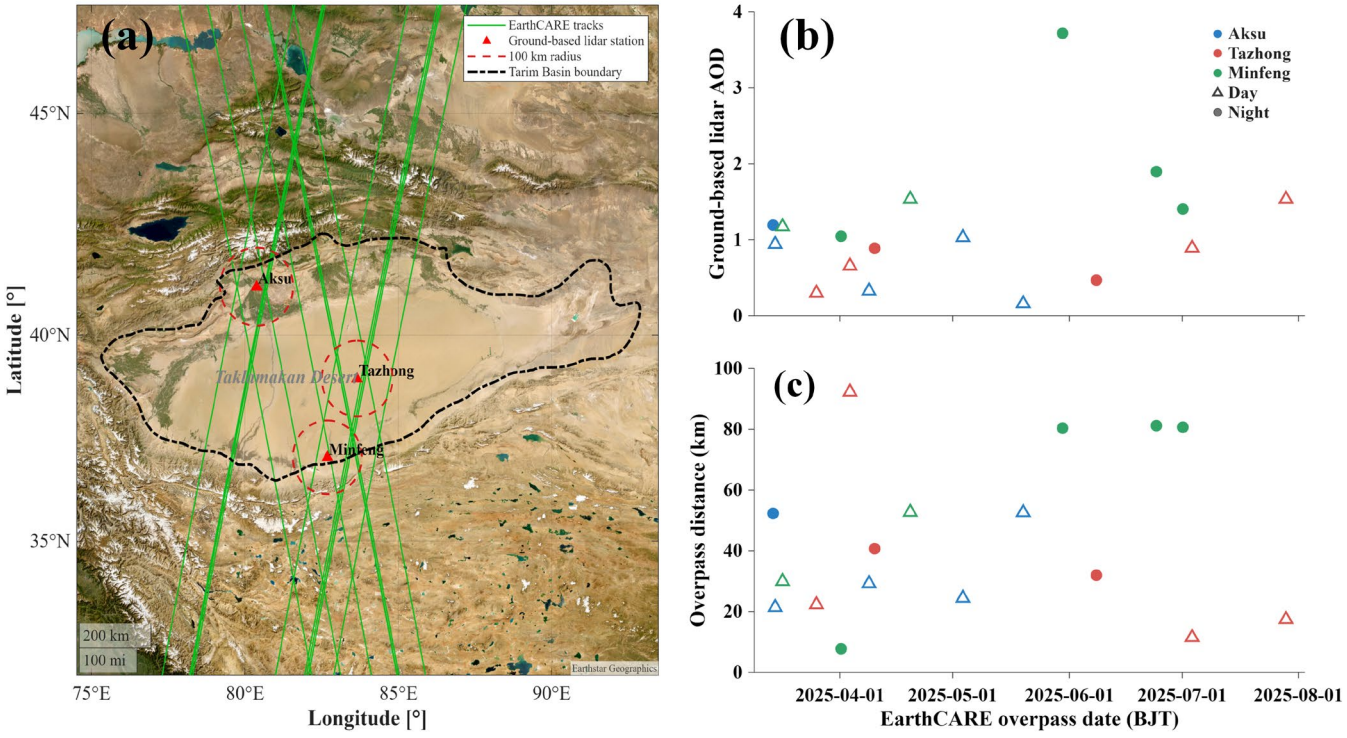


Figure 1 Spatial and temporal characteristics of the 17 overpass collocation cases examined in this study. (a) EarthCARE ground tracks (green lines), ground-based lidar stations (red triangles), 100 km collocation domains around the stations (red dashed circles), and the Tarim Basin boundary (black dash-dotted line). (b) Ground-based lidar-derived AOD for each case. (c) Horizontal distance between each station and its closest ATLID profile. In panels (b) and (c), blue, red, and green represent Aksu, Tazhong, and Minfeng, respectively; open triangles and filled circles indicate daytime and nighttime overpasses. All times are expressed in Beijing time (BJT, UTC+8). © Esri, Maxar, Earthstar Geographics, and the GIS User Community | Powered by Esri.

3.2 Capability of ATLID to capture dust vertical structures

3.2.1 Satellite–ground observations of dust vertical structure over Aksu

On 14 March 2025, EarthCARE passed near the Aksu station, with a minimum distance of approximately 52.5 km between its ground track and the station (Fig. 2a). Located on the northwestern margin of the Taklamakan Desert, the Aksu station provided an opportunity to compare the aerosol vertical structure and optical properties observed by spaceborne and ground-based lidars during this overpass. All heights are reported above sea level, and all times are given in UTC+8. Continuous ground-based lidar observations revealed pronounced diurnal variations in the aerosol layer (Fig. 2c, e, and g). From the early morning hours until dawn, the aerosol layer extended to approximately 5 km, with stronger extinction and backscatter signals concentrated at lower altitudes and relatively weak scattering layers above. The aerosol layer top subsequently descended, remaining mostly below approximately 2 km during the daytime before rising again at night. During the satellite overpass, ATLID also detected enhanced extinction and backscatter signals at lower altitudes. The height, intensity, and vertical extent of the aerosol layer varied considerably along the satellite track, indicating spatial heterogeneity in the atmospheric structure

https://doi.org/10.5194/egusphere-2026-6659
Preprint. Discussion started: 22 November 2026
© Author(s) 2026. CC BY 4.0 License.

across the overpass region (Fig. 2b, d, and f). Comparison of the vertical profiles showed good agreement between the two lidars in the altitude of the main aerosol layer and the vertical variations in extinction and backscatter coefficients (Fig. 2h and i). Both observations exhibited pronounced peaks near 2 km, with peak extinction coefficients of approximately 0.9–1.0 km^{-1} and peak backscatter coefficients of approximately 0.016–0.019 km^{-1} sr^{-1}. Above these peaks, both optical parameters generally decreased with increasing altitude and were substantially weaker at approximately 4 km. Compared with the ground-based observations, ATLID generally yielded higher extinction and backscatter coefficients between approximately 2 and 3 km, whereas the ground-based profiles exhibited more pronounced local vertical fluctuations. In addition, ATLID detected a distinct elevated scattering layer at approximately 8.5–9.5 km, indicating the presence of multiple scattering layers within the satellite sampling region. The differences between the spaceborne and ground-based depolarization ratios were more pronounced than those in extinction and backscatter coefficients (Fig. 2j). Between approximately 2 and 4 km, the ATLID depolarization ratio remained around 0.30–0.33, while the ground-based values were generally lower and exhibited greater vertical variability. The relatively high depolarization ratios indicate a substantial contribution from nonspherical particles. Given the proximity of the Aksu station to the Taklamakan Desert, these optical characteristics are consistent with dust aerosols. Overall, the spaceborne and ground-based observations consistently captured the main vertical structure of the lower aerosol layer in this case, although differences remained in the magnitudes of the optical parameters, particularly the depolarization ratio. Considering the spatial separation of approximately 52.5 km and the pronounced along-track variations in atmospheric structure, these differences may reflect the combined effects of spatial heterogeneity, sampling and averaging procedures, and retrieval methods.

https://doi.org/10.5194/egusphere-2026-6659
Preprint. Discussion started: 22 November 2026
© Author(s) 2026. CC BY 4.0 License.

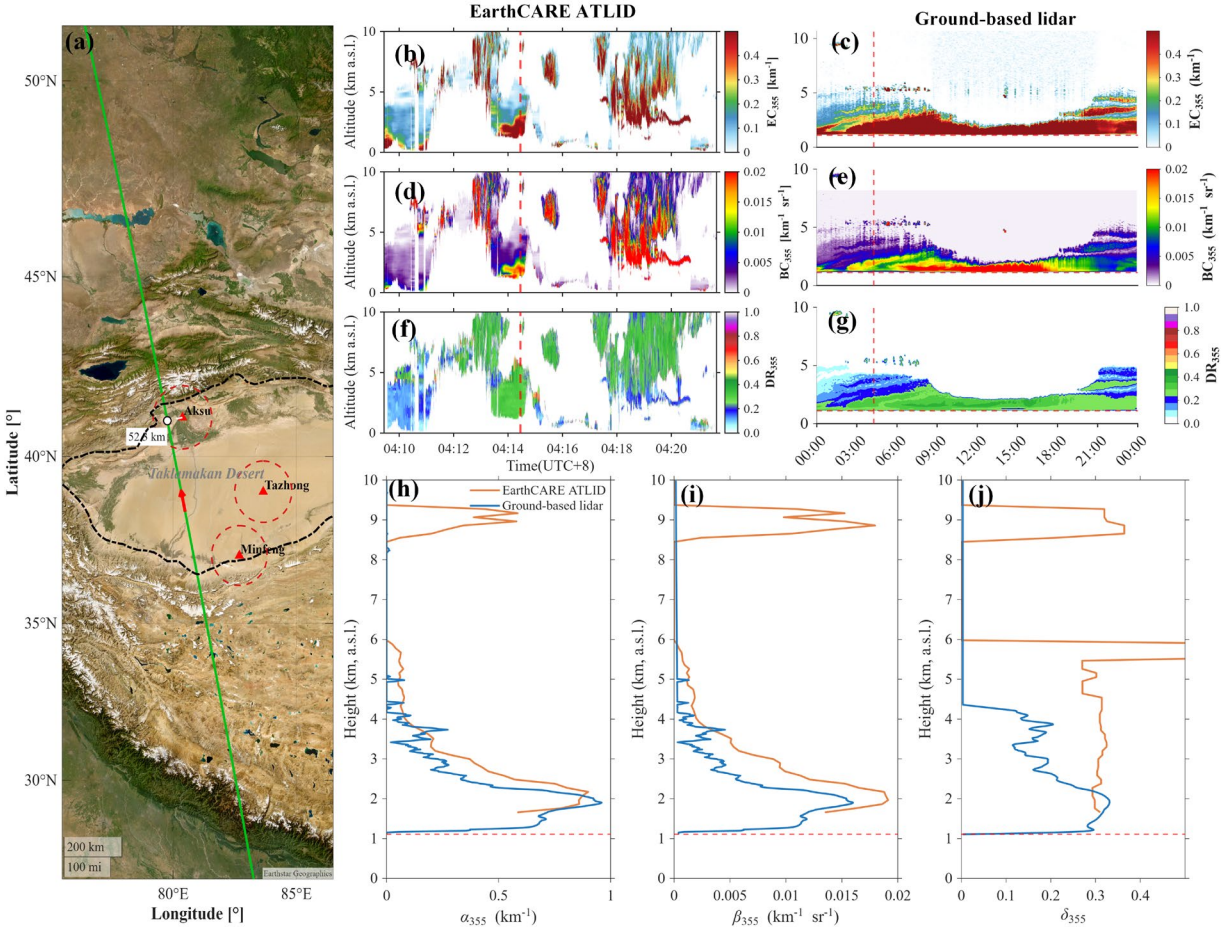


Figure 2 Comparison of EarthCARE ATLID and ground-based lidar observations over Aksu on 14 March 2025. (a) EarthCARE ground track (green line), lidar stations (red triangles), and 100 km sampling radii (red dashed circles). The red arrow indicates the satellite flight direction, and the white circle marks the satellite profile closest to Aksu, approximately 52 km from the station. The black dash-dotted line outlines the Tarim Basin. (b, d, f) Along-track distributions of the extinction coefficient, backscatter coefficient, and particle linear depolarization ratio at 355 nm measured by ATLID. (c, e, g) Corresponding time–height distributions observed by the ground-based lidar at Aksu. Vertical red dashed lines indicate the satellite's closest approach to the station. (h–j) Comparisons of the matched extinction, backscatter, and depolarization profiles, with orange and blue lines representing ATLID and ground-based lidar observations, respectively. Horizontal red dashed lines indicate the station altitude (1107.1 m a.s.l.). All times are UTC+8, and heights are expressed above sea level. © Esri, Maxar, Earthstar Geographics, and the GIS User Community | Powered by Esri.

3.2.2 Satellite–ground observations of dust vertical structure over Tazhong and Minfeng

On 24 June 2025, EarthCARE passed over the Taklamakan Desert, while ground-based lidars at Minfeng and Tazhong observed dust layers during the overpass. The minimum distances between the satellite ground track and the two stations were approximately 81.1 km and 45.5 km, respectively (Fig. 3a). Minfeng is located on the southern margin of the desert, whereas Tazhong lies in its interior. Observations from these two locations provided complementary references for evaluating the dust vertical structure and optical properties detected by ATLID. All heights are reported above sea level, and all times are given in UTC+8. The ATLID along-track observations showed that dust in the track segments corresponding to Minfeng and

https://doi.org/10.5194/egusphere-2026-6659
Preprint. Discussion started: 22 November 2026
© Author(s) 2026. CC BY 4.0 License.

Tazhong was primarily distributed between approximately 1 and 5 km, characterized by enhanced extinction, backscatter, and depolarization signals (Fig. 3b–d). The intensity, thickness, and vertical distribution of the dust layer varied considerably along the track, indicating spatial heterogeneity during this event. The enhanced lower-level extinction and backscatter signals indicated substantial dust contributions to optical attenuation and scattering, while the elevated depolarization ratios reflected the nonspherical nature of dust particles. Distinct strong scattering structures were also present at middle and upper levels and should be analyzed separately from the lower-level dust. At Minfeng, dust was mainly distributed between approximately 1.5 and 5 km from the early morning hours until dawn, with stronger extinction and backscatter signals concentrated in the lower and middle portions of the layer (Fig. 3e and g). Over time, the upper boundary of the strong scattering layer descended, the dust layer became thinner, and the extinction and backscatter signals weakened markedly around noon. At Tazhong, lower-level dust was also observed during the satellite overpass, but its vertical distribution exhibited more pronounced layering (Fig. 3f and h). The stronger dust scattering signals gradually weakened during the daytime, while weak scattering layers extending to higher altitudes persisted into the afternoon and night. Together, the two stations showed strong lower-level optical signals during the early morning hours, alongside differences in the vertical structure and evolution of dust between the desert margin and interior. The depolarization ratios further revealed the optical characteristics of this dust event and the differences between the two stations (Fig. 3i and j). Tazhong exhibited more pronounced depolarization enhancement during the early morning hours and the satellite overpass, whereas depolarization ratios within the dust layer at Minfeng were generally lower. These differences suggest that, although both stations were affected by dust, particle shape, size distribution, or the degree of mixing with other aerosols may have differed. The available observations alone cannot distinguish the individual contributions of these factors. ATLID also detected enhanced lower-level depolarization in the corresponding track segments, consistent with the nonspherical dust particle characteristics identified by the ground-based observations. Overall, the observations from both stations provided qualitative support for ATLID's identification of the main altitude range and optical characteristics of dust layers over the Taklamakan Desert. They also revealed substantial spatial differences in dust between the desert margin and interior. Given the spatial separation between the satellite track and the stations, together with the along-track variability in dust layer structure, differences between the spaceborne and ground-based observations should be interpreted in terms of spatial representativeness. Quantitative agreement in the optical parameters requires further evaluation using profile comparisons under consistent spatial and temporal matching criteria.

https://doi.org/10.5194/egusphere-2026-6659
Preprint. Discussion started: 22 November 2026
© Author(s) 2026. CC BY 4.0 License.

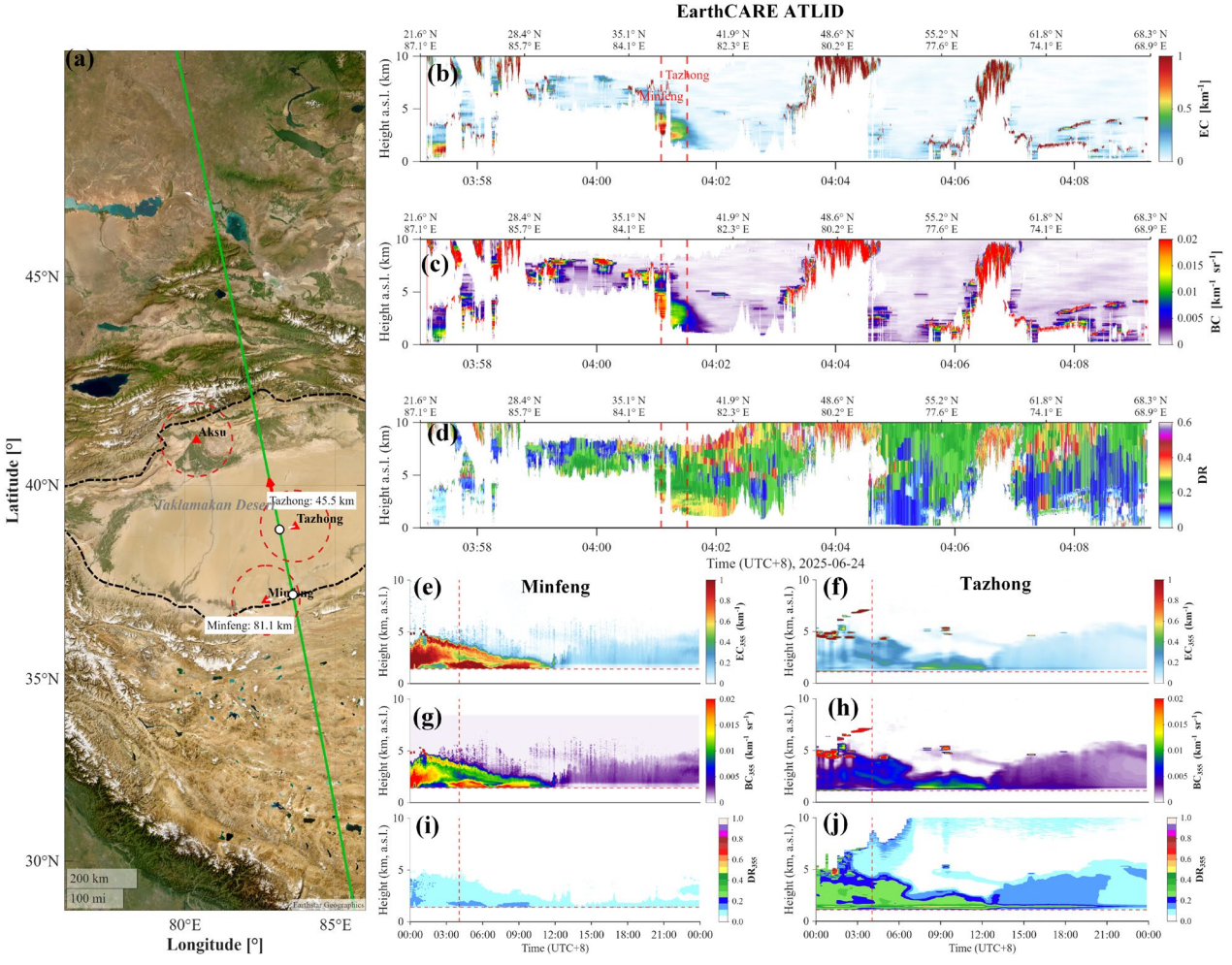


Figure 3 Evaluation of EarthCARE ATLID using coordinated observations from the Minfeng and Tazhong lidar stations during a dust event over the Taklamakan Desert on 24 June 2025. (a) EarthCARE ground track (green line) and ground-based lidar station locations (red triangles). Minfeng and Tazhong are located on the southern desert margin and in the desert interior, respectively, with minimum distances of approximately 81.1 and 45.5 km from the satellite ground track. Together, the two stations provide complementary observations for evaluating the dust vertical structure and optical properties retrieved by ATLID. (b–d) ATLID along-track extinction coefficient, backscatter coefficient, and depolarization ratio at 355 nm. Red dashed vertical lines mark the along-track positions corresponding to the two stations. (e–j) Time–height distributions of extinction coefficient (e, f), backscatter coefficient (g, h), and depolarization ratio (i, j) at Minfeng (left column) and Tazhong (right column). Red dashed vertical lines indicate the satellite overpass time corresponding to each station, and red dashed horizontal lines indicate station elevations. All heights are above sea level, and all times are in UTC+8. © Esri, Maxar, Earthstar Geographics, and the GIS User Community | Powered by Esri.

Figure 4 compares the optical parameter profiles from ATLID and the ground-based lidars at Minfeng and Tazhong during the dust event on 24 June 2025. At Minfeng, both observations detected pronounced dust signals between approximately 1.5 and 4.5 km, but differences were evident in peak altitude and layer structure (Fig. 4a and b). ATLID exhibited a prominent peak near 2.7 km, whereas the ground-based observations showed local enhancements near 1.8 and 3.7 km. Between approximately 2 and 4 km, ATLID depolarization ratios ranged from approximately 0.25 to 0.40, substantially exceeding the ground-based

https://doi.org/10.5194/egusphere-2026-6659
Preprint. Discussion started: 22 November 2026
© Author(s) 2026. CC BY 4.0 License.

values of around 0.10 (Fig. 4c). In contrast, the extinction and backscatter profiles at Tazhong agreed more closely with ATLID. Both observations identified a dust layer extending from approximately 1 to 4.5 km, with enhanced signals near 2.5–3 km, and their depolarization ratios were also more comparable (Fig. 4d–f). The observations from both stations indicate that ATLID captured the main vertical structure of this dust event, although agreement between the spaceborne and ground-based observations differed considerably between stations. Tazhong, located closer to the satellite ground track (45.5 km), showed better profile agreement than Minfeng (81.1 km), suggesting that spatial representativeness may influence the validation results. However, these differences may also reflect the combined effects of dust spatial heterogeneity, particle properties, and sampling and retrieval methods, and therefore cannot be attributed solely to the matching distance.

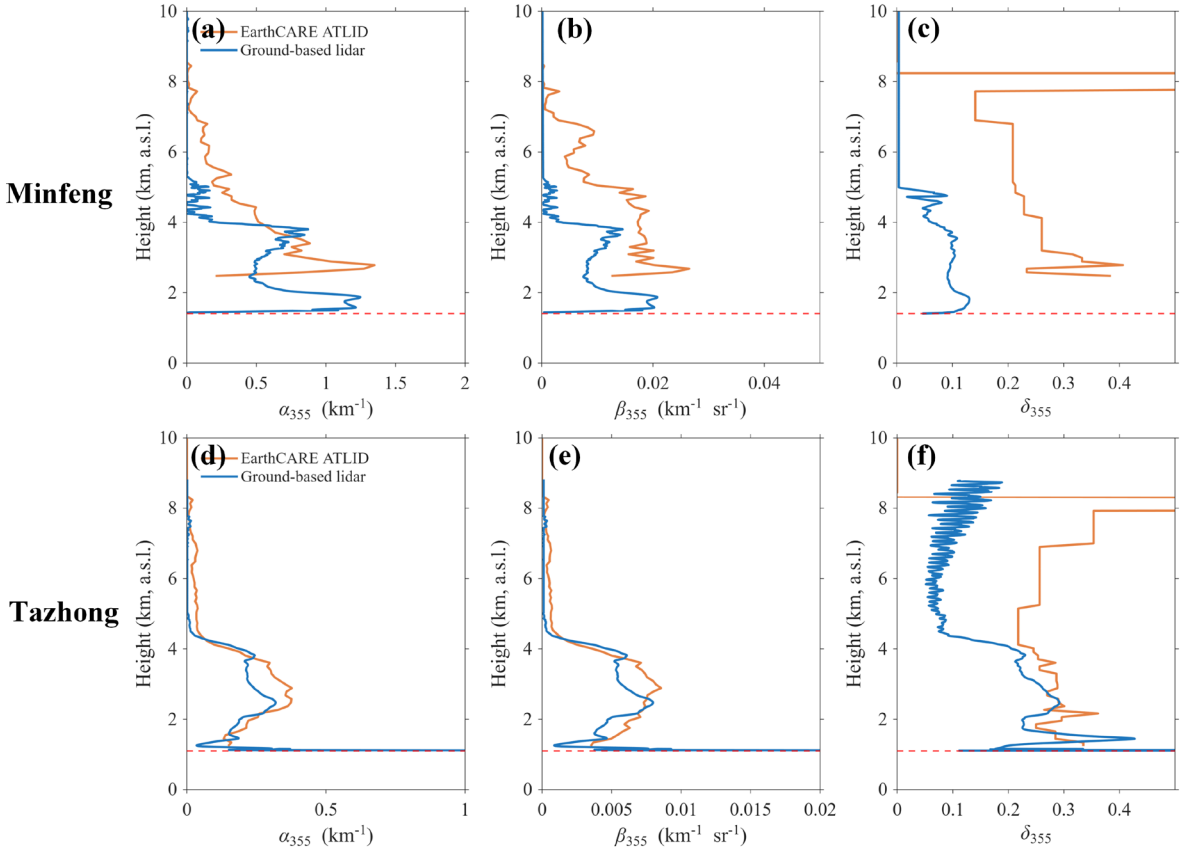


Figure 4 Comparison of vertical profiles of optical parameters at 355 nm between EarthCARE ATLID and ground-based lidars at Minfeng and Tazhong during the dust event on 24 June 2025. (a–c) Extinction coefficient (α_{355}), backscatter coefficient (β_{355}), and depolarization ratio (δ_{355}) at Minfeng; (d–f) corresponding optical parameters at Tazhong. Orange and blue solid lines represent ATLID and ground-based lidar results, respectively. Red dashed horizontal lines indicate station elevations. All heights are above sea level.

3.3 Multi-site evaluation of ATLID aerosol optical properties

Figure 5 compares the optical parameters retrieved by ATLID and the ground-based lidars at Aksu, Tazhong, and Minfeng. Extinction coefficients exhibited positive correlations of 0.88, 0.81, and 0.69, respectively (Fig. 5a–c). ATLID generally

https://doi.org/10.5194/egusphere-2026-6659
Preprint. Discussion started: 22 November 2026
© Author(s) 2026. CC BY 4.0 License.

yielded higher extinction values, with mean biases of 0.077, 0.108, and 0.079 km^{-1} and mean bias percentages (MBPs) of 27.5%, 48.0%, and 17.6%, respectively. These results indicate that ATLID reproduced much of the observed extinction variability, although positive offsets remained at all three stations. Backscatter agreement varied more substantially among stations, with correlation coefficients of 0.36, 0.87, and 0.62 at Aksu, Tazhong, and Minfeng, respectively (Fig. 5d–f). Tazhong showed the strongest correlation, whereas Aksu exhibited greater scatter and weaker correspondence. Mean backscatter biases were positive at all three stations, reaching 0.0075, 0.0049, and 0.0059 km^{-1} sr^{-1}, with corresponding MBPs of 159.5%, 72.3%, and 83.2%. Thus, even the strong correlation at Tazhong was accompanied by a substantial positive percentage bias, emphasizing the distinction between agreement in variability and agreement in magnitude. Particle linear depolarization ratios showed substantially poorer correspondence (Fig. 5g–i). Aksu exhibited a negative correlation of −0.52, while correlations at Tazhong and Minfeng were close to zero, at 0.09 and -0.02, respectively. ATLID values were frequently clustered around 0.3 and did not consistently reproduce the variations observed by the ground-based lidars. Mean biases were 0.199, 0.148, and 0.214, with MBPs of 144.8%, 95.1%, and 300.3%, respectively. Overall, extinction showed more consistent positive correlations across stations, backscatter agreement was strongly station dependent, and depolarization ratios exhibited limited correspondence and persistent positive biases.

https://doi.org/10.5194/egusphere-2026-6659
Preprint. Discussion started: 22 November 2026
© Author(s) 2026. CC BY 4.0 License.

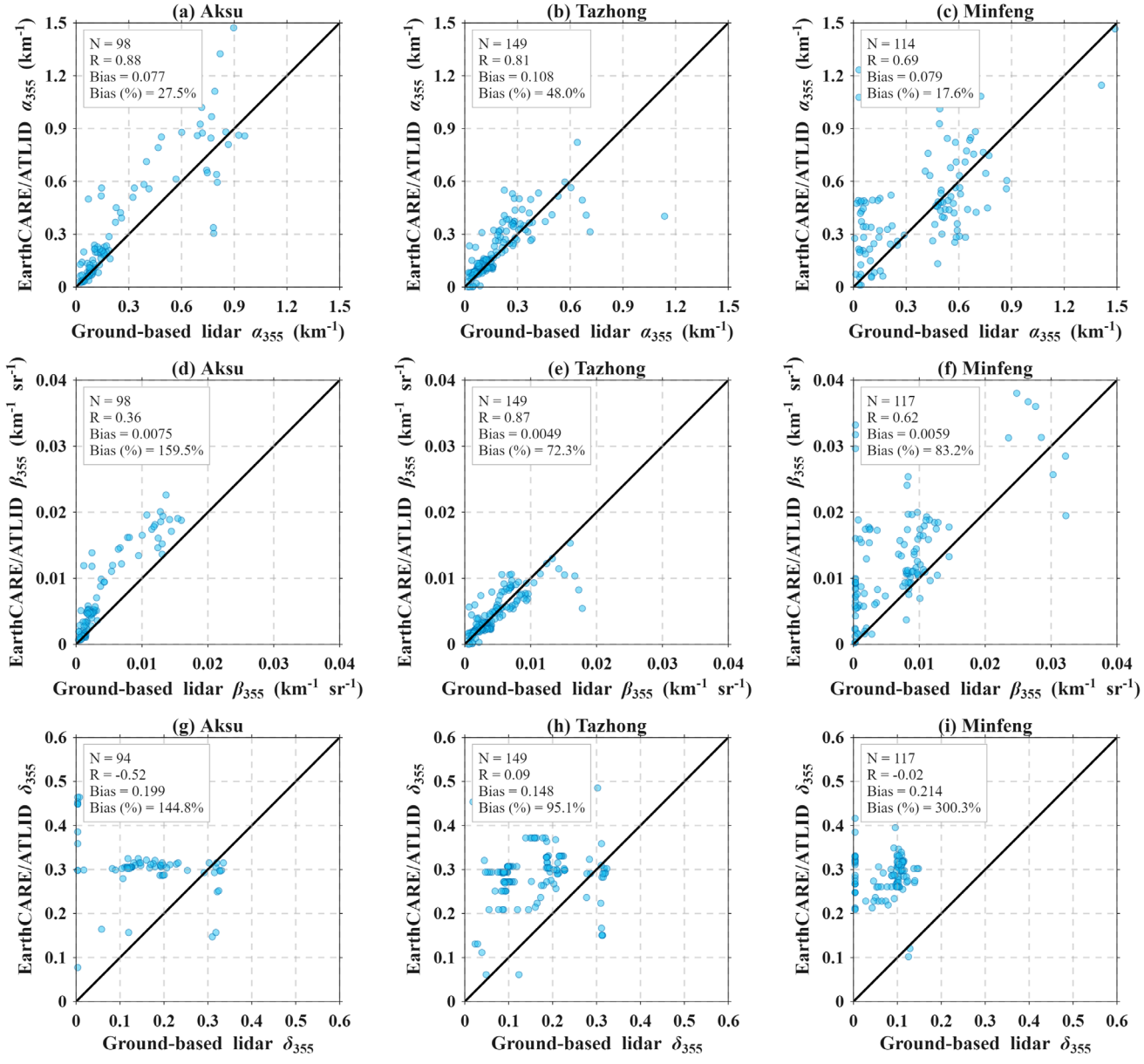


Figure 5 Statistical comparisons of optical parameters at 355 nm between EarthCARE ATLID and ground-based lidars at Aksu, Tazhong, and Minfeng. (a–c) Extinction coefficient (α_{355}); (d–f) backscatter coefficient (β_{355}); and (g–i) depolarization ratio ($\beta\delta_{355}$). The left, middle, and right columns correspond to Aksu, Tazhong, and Minfeng, respectively.

Figure 6 presents the vertical distributions of biases in ATLID optical parameters relative to ground-based lidar observations. Positive biases in extinction and backscatter coefficients were primarily concentrated at lower and middle levels and differed among stations (Fig. 6a–f). At Aksu, pronounced positive biases occurred between approximately 2 and 4 km, accompanied by broad interquartile ranges, indicating substantial variability among matched samples. At Tazhong, the median biases in both parameters were generally closer to zero, although positive biases remained at some lower levels. At Minfeng, extinction

https://doi.org/10.5194/egusphere-2026-6659
Preprint. Discussion started: 22 November 2026
© Author(s) 2026. CC BY 4.0 License.

biases were slightly negative near 2 km but predominantly positive between approximately 3 and 5.5 km; backscatter coefficients were also overestimated over a similar altitude range. Above approximately 6 km, extinction and backscatter biases generally approached zero at all three stations. However, this pattern may also reflect weaker scattering signals at higher altitudes and does not, by itself, demonstrate improved relative agreement. Positive biases in depolarization ratios extended over broader altitude ranges, with distinct vertical patterns among the three stations (Fig. 6g–i). At Aksu, positive biases were mainly concentrated between approximately 2 and 6 km, whereas at Tazhong they extended to approximately 8 km. Minfeng exhibited persistent positive biases between approximately 2 and 7.5 km, with larger values near 6–7 km. The interquartile ranges broadened substantially at some altitudes, particularly between approximately 7 and 9 km at Tazhong, indicating greater variability in depolarization differences at these levels. Overall, extinction and backscatter biases were primarily concentrated within the lower-level aerosol layers, whereas depolarization biases covered broader vertical ranges, consistent with the generally positive biases and weak correlations shown in Fig. 5.

https://doi.org/10.5194/egusphere-2026-6659
Preprint. Discussion started: 22 November 2026
© Author(s) 2026. CC BY 4.0 License.

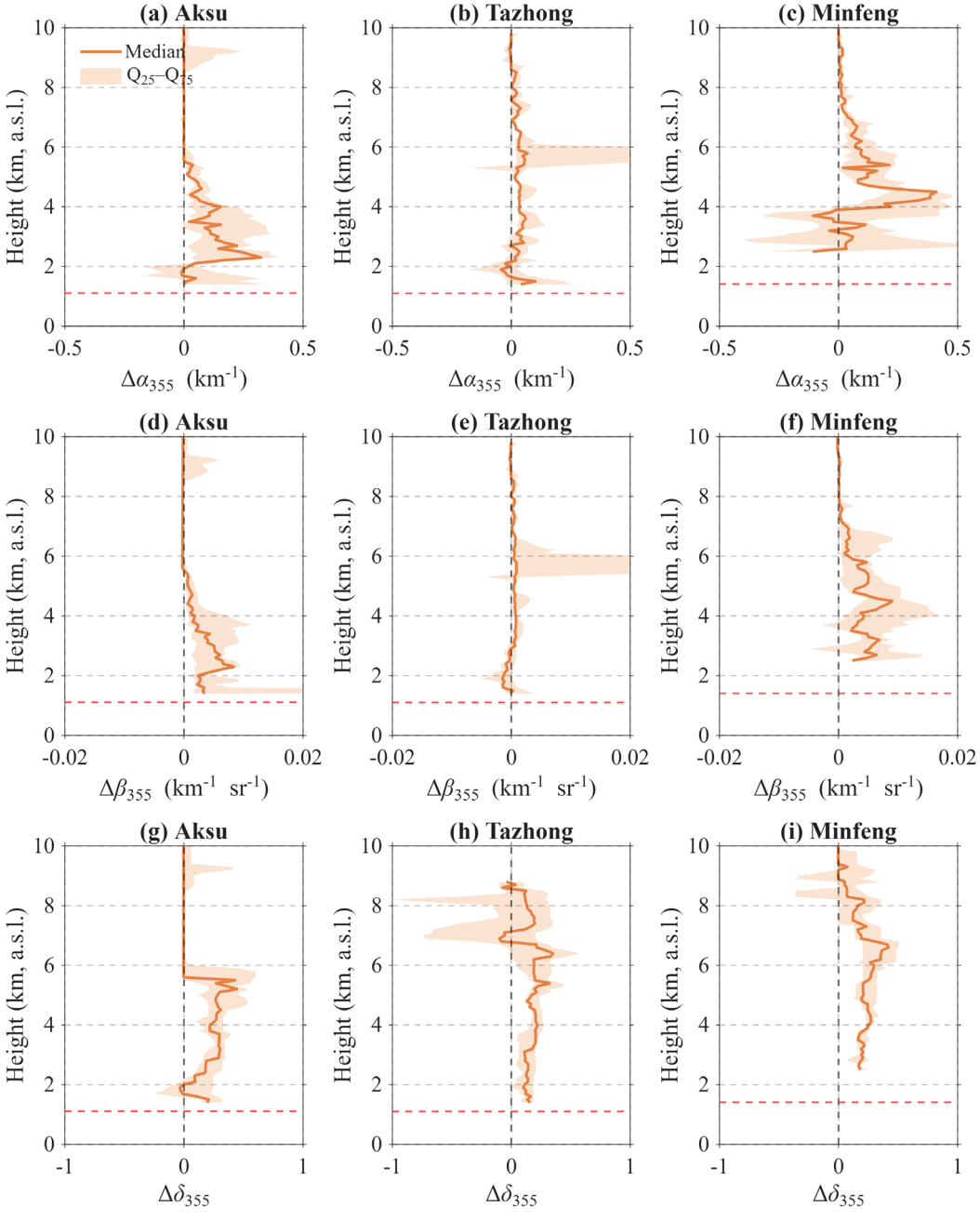


Figure 6 Vertical distributions of biases in optical parameters at 355 nm from EarthCARE ATLID relative to ground-based lidars at Aksu, Tazhong, and Minfeng. (a–c) Extinction coefficient bias ($\Delta\alpha_{355}$); (d–f) backscatter coefficient bias ($\Delta\beta_{355}$); and (g–i) depolarization ratio bias ($\Delta\delta_{355}$). The left, middle, and right columns correspond to Aksu, Tazhong, and Minfeng, respectively. Bias is defined as the ATLID value minus the ground-based lidar value. Orange solid lines indicate the median bias at each altitude, and light orange shading represents the 25th–75th percentile range ($Q_{25} - Q_{75}$). Gray dashed vertical lines indicate zero bias, and red dashed horizontal lines denote station elevations. All heights are above sea level.

https://doi.org/10.5194/egusphere-2026-6659
Preprint. Discussion started: 22 November 2026
© Author(s) 2026. CC BY 4.0 License.

3.4 Case-based assessment of ATLID lidar ratio using nighttime Raman observations

Figure 7 compares the vertical profiles retrieved by EarthCARE/ATLID and the ground-based Raman lidar at Tazhong on 8 June 2025 at 03:59 BJT. Both instruments capture the overall decrease in extinction and backscatter with altitude, although differences are evident in the resolved vertical structures. The Raman lidar extinction profile exhibits pronounced enhancements at approximately 1.8 and 5.7 km ASL, reaching about 0.4 and 0.3 km^{-1}, respectively. These features are substantially weaker in the ATLID profile, which varies more gradually with altitude. Backscatter profiles agree more closely over approximately 2–5 km ASL, whereas the narrow enhancement observed by the ground-based lidar near 5.9 km ASL is not reproduced by ATLID. Larger differences are evident in particle linear depolarization ratio and lidar ratio. The ground-based depolarization ratio remains around 0.08–0.10 over much of the 2–5 km ASL interval, compared with approximately 0.25–0.30 for ATLID. ATLID also retains higher depolarization ratios above this interval, indicating a persistent positive difference throughout most of the displayed profile. The ATLID lidar ratio remains relatively stable, generally around 45–55 sr, whereas the Raman-derived lidar ratio exhibits more pronounced vertical variability, including several sharp enhancements. Overall, this case shows closer agreement in the broad backscatter structure than in extinction, depolarization ratio, and lidar ratio, while the ground-based Raman lidar resolves vertical features that are less apparent in the ATLID profiles at their original resolutions.

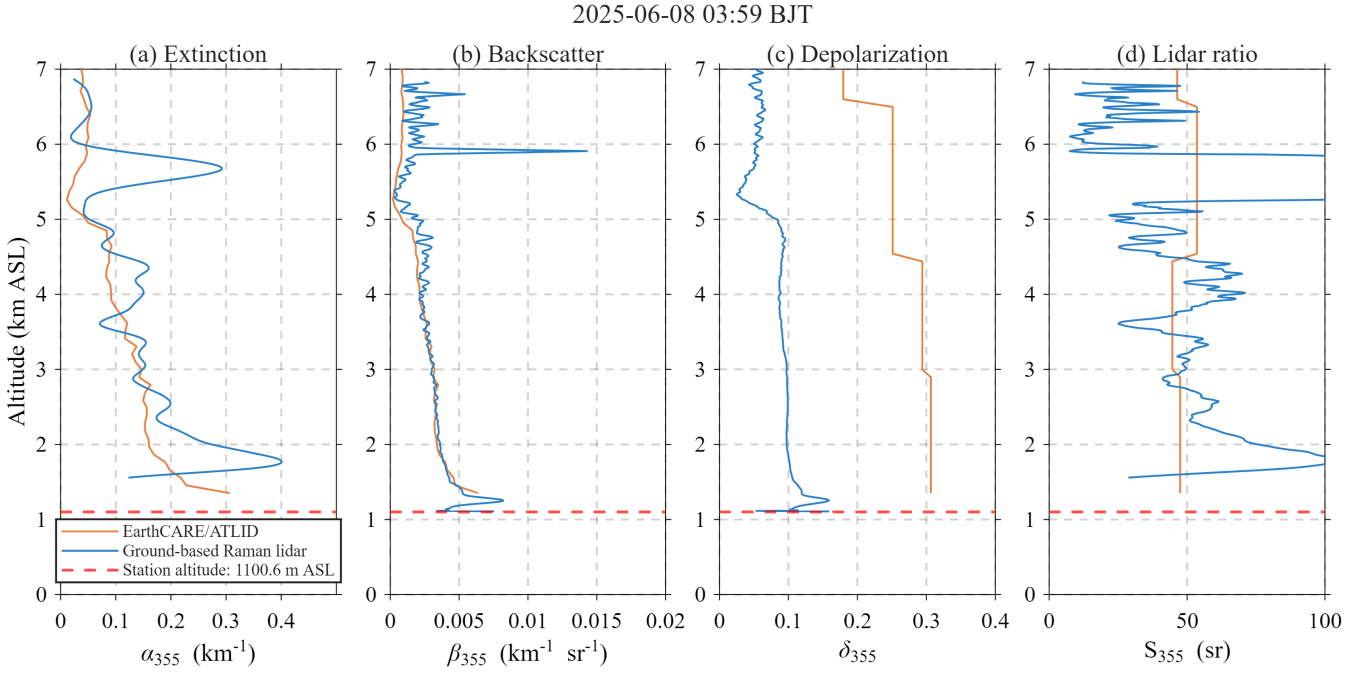


Figure 7 Comparison of vertical profiles of (a) extinction coefficient, (b) backscatter coefficient, (c) particle linear depolarization ratio, and (d) lidar ratio at 355 nm retrieved by EarthCARE/ATLID (orange) and the ground-based Raman lidar (blue) at Tazhong on 8 June 2025 at 03:59 Beijing time (BJT, UTC+8). Altitudes are referenced to mean sea level (ASL), and the red dashed horizontal line marks the station elevation of 1100.6 m ASL.

https://doi.org/10.5194/egusphere-2026-6659
Preprint. Discussion started: 22 November 2026
© Author(s) 2026. CC BY 4.0 License.

3.5 Dependence of retrieval performance on dust load

Figure 8 shows the mean biases in extinction coefficient (EC), backscatter coefficient (BC), and particle linear depolarization ratio (DR) as a function of horizontal distance and ground-based AOD at the three stations. Positive biases dominate all three parameters, with negative biases limited to a few comparisons. EC and BC exhibit broadly similar patterns of bias magnitude across the distance–AOD space, whereas DR generally shows larger biases. The sampled conditions differ among stations, with the higher-AOD cases occurring mainly at Minfeng. Bias magnitude does not increase consistently with either horizontal distance or AOD. Relatively large biases occur at short distances and low AOD, while some more distant comparisons exhibit small biases. A particularly large DR bias occurs at a distance of approximately 40 km and an AOD of approximately 0.9. In contrast, the highest-AOD case exhibits small EC and BC biases, although its DR bias remains appreciable. These results suggest that close spatial coincidence and low aerosol loading alone do not ensure small satellite–ground differences. Overall, within the sampled ranges, the biases show no clear monotonic dependence on horizontal distance or aerosol loading.

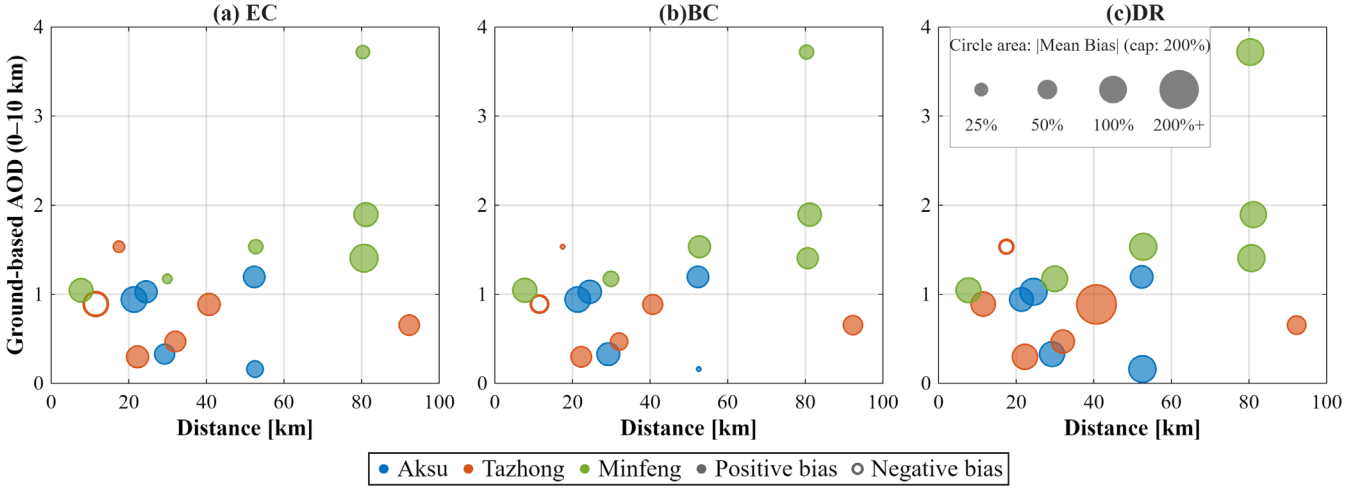


Figure 8 Dependence of the mean biases in (a) extinction coefficient (EC), (b) backscatter coefficient (BC), and (c) particle linear depolarization ratio (DR) on the horizontal distance between the ATLID ground track and the ground-based lidar station and the ground-based aerosol optical depth (AOD), integrated over 0–10 km above ground level. Each circle represents one overpass comparison. Blue, orange, and green denote Aksu, Tazhong, and Minfeng, respectively. Circle area is proportional to the absolute mean bias, with values exceeding 200% displayed using the size corresponding to 200%. Filled and open circles indicate positive and negative biases, respectively.

4 Discussions

4.1 EarthCARE's ability to capture the vertical structure of dust aerosols

The case studies and statistical comparisons across the three stations demonstrate that the EarthCARE/ATLID L2A A-EBD product can capture the altitude ranges and overall vertical structure of the main dust layers over the Taklamakan Desert. However, differences remain in local peaks, fine-scale layering, and optical parameter magnitudes, indicating that the ability to identify major layer structures should be assessed separately from quantitative retrieval accuracy. ATLID's high-spectral-

https://doi.org/10.5194/egusphere-2026-6659
Preprint. Discussion started: 22 November 2026
© Author(s) 2026. CC BY 4.0 License.

resolution design separates particulate and molecular backscatter signals, providing observational constraints for extinction and backscatter retrievals (Wehr et al., 2023). The agreement in major dust-layer locations observed here is consistent with this capability, whereas the weaker extinction peaks and narrow-layer enhancements in A-EBD during the Raman lidar case on 8 June 2025 illustrate that agreement in overall structure does not necessarily imply agreement in local optical intensity. Recent PollyNET validation similarly found that A-EBD reproduced aerosol vertical structure well in most evaluated scenarios, while quantitative performance differed among parameters, with substantial aerosol depolarization-ratio discrepancies in processing baselines BA and BB (Baars et al., 2026). These findings are consistent with the weaker agreement in particle linear depolarization ratio (LPDR) observed in this study, although comparisons should account for the processing baseline used. Because the EarthCARE HETEAC framework uses lidar ratio and LPDR to characterize aerosol types and mixtures, uncertainties in depolarization ratio may also affect the interpretation of dust properties (Wandinger et al., 2023). The present results therefore primarily support the use of extinction and backscatter profiles to investigate dust-layer structure and vertical distribution, whereas quantitative inferences about dust fraction or mixing state from LPDR require further validation.

4.2 Sources of differences between EarthCARE and ground-based lidar profiles

Differences between EarthCARE and ground-based lidar profiles may reflect the combined effects of spatiotemporal representativeness, effective resolution, and retrieval uncertainties. In this study, the ATLID profile closest to each ground station was paired with the ground-based profile nearest in time to its acquisition. However, this nearest-neighbor matching does not guarantee that the two systems sampled the same air mass. Differences in dust intensity, layering, and evolution between Minfeng and Tazhong indicate that substantial spatial heterogeneity can occur within the same regional dust event. This interpretation is consistent with previous studies emphasizing the importance of target homogeneity for satellite–ground comparisons, particularly within the boundary layer, where local processes can strongly influence aerosol distributions (Floutsi et al., 2026; Mamouri et al., 2009). Selecting the nearest profile also does not eliminate differences in effective resolution arising from smoothing within the processing chain. A-FM-guided smoothing, together with the prior constraints and assumption of a constant lidar ratio within each identified layer in A-EBD, may influence the representation of local peaks and layer boundaries (Donovan et al., 2024; Van Zadelhoff et al., 2023). Residual cloud contamination, signal attenuation, and uncertainties in multiple-scattering corrections may further affect the comparisons. For LPDR, signal quality and polarization calibration in both systems also require consideration (Freudenthaler, 2016). The results further show that, within the sampled ranges, satellite–ground biases exhibit no clear monotonic dependence on horizontal distance or ground-based AOD. Relatively large biases occur even at short distances and low aerosol loading, indicating that neither distance nor loading alone adequately explains the observed differences. Physically, higher dust loading may strengthen particulate backscatter while also increasing attenuation along the propagation path; its net effect on retrieval performance therefore depends on dust-layer structure and observational conditions. In the highest-AOD case, the mean extinction and backscatter biases were small, whereas the LPDR bias remained appreciable, further demonstrating that higher loading does not necessarily correspond to larger satellite–ground biases and that responses differ among parameters. Nevertheless, the limited sample size and the

https://doi.org/10.5194/egusphere-2026-6659
Preprint. Discussion started: 22 November 2026
© Author(s) 2026. CC BY 4.0 License.

concentration of high-AOD events at Minfeng prevent a clear separation of the effects of distance, loading, and site-specific conditions, requiring further evaluation using additional independent events.

4.3 Implications, limitations, and future perspectives

Although this study is based on observations from three ground-based lidar stations and a limited number of collocated dust events, it provides initial observational evidence that EarthCARE/ATLID can capture the dominant vertical structure of dust aerosols over the Taklamakan Desert. Reliable satellite-derived profiles of dust vertical structure are essential for investigating dust uplift, vertical transport, downwind export, and dust–radiation–cloud interactions at regional and larger scales. These findings therefore support the future use of EarthCARE aerosol products in studies of dust-related processes, particularly those focusing on aerosol layer structure and vertical distribution. Nevertheless, several limitations should be acknowledged. First, validation using three ground-based lidar stations cannot fully represent the pronounced spatial heterogeneity of dust vertical structure across the Taklamakan Desert. Second, the limited number of collocated dust events constrains the statistical robustness of the findings and precludes a comprehensive assessment of seasonal variability and differences among events. Accordingly, these results should be regarded as a preliminary assessment of ATLID performance during satellite overpasses coinciding with dust events, rather than a comprehensive characterization of its performance across all dust conditions. Future work should extend the observation period, include more collocated satellite overpasses, and incorporate additional ground-based lidar stations covering a wider range of dust environments. Furthermore, stratifying cases by dust intensity, cloud influence, and atmospheric stability would help identify the conditions under which ATLID performs best and those associated with the greatest uncertainty. Particular attention should be given to depolarization-related products, as the weaker agreement in LPDR indicates that further evaluation is needed before these products can be used to quantitatively infer particle nonsphericity and dust microphysical properties.

5 Conclusions

This study evaluated aerosol optical profiles from the EarthCARE/ATLID L2A A-EBD product over the Taklamakan Desert using ground-based lidar observations at Aksu, Tazhong, and Minfeng during spring and summer 2025. The main conclusions are as follows:

(1) ATLID generally identified the main altitude ranges and vertical structures of dust layers, but quantitative agreement with ground-based observations varied among optical parameters and stations. The correlation coefficients for extinction were 0.88, 0.81, and 0.69 at Aksu, Tazhong, and Minfeng, respectively, with corresponding mean bias percentages (MBPs) of 27.5%, 48.0%, and 17.6%. For backscatter, the correlation coefficients were 0.36, 0.87, and 0.62, with MBPs of 159.5%, 72.3%, and 83.2%, respectively. Both parameters were generally overestimated at all three stations, and higher correlations did not necessarily correspond to smaller biases. Agreement in particle linear depolarization ratio was weaker: Aksu exhibited a negative correlation ($R = -0.52$), while the correlations at Tazhong and Minfeng were 0.09 and −0.02, respectively. Mean

https://doi.org/10.5194/egusphere-2026-6659
Preprint. Discussion started: 22 November 2026
© Author(s) 2026. CC BY 4.0 License.

biases were 0.199, 0.148, and 0.214, with MBPs of 144.8%, 95.1%, and 300.3%, respectively. These results indicate that ATLID extinction coefficients maintained relatively strong positive correlations with ground-based observations across all three stations, whereas backscatter agreement was strongly station dependent and depolarization ratios showed limited correspondence with ground-based variability.

(2) The biases exhibited distinct vertical patterns. Positive extinction and backscatter biases were mainly concentrated within aerosol layers at lower and middle altitudes, particularly at approximately 2–4 km at Aksu and 3–5.5 km at Minfeng, while median biases at Tazhong were generally closer to zero. Above approximately 6 km, absolute biases in both parameters generally decreased, although this did not necessarily indicate improved relative agreement. Positive depolarization ratio biases extended over broader altitude ranges. The nighttime Raman lidar comparison at Tazhong further showed closer agreement in the overall backscatter structure, whereas larger differences remained in extinction, depolarization ratio, and lidar ratio.

(3) Within the sampled ranges, bias magnitude showed no clear systematic relationship with either horizontal distance or aerosol loading. Shorter collocation distances or lower AOD did not necessarily correspond to smaller satellite–ground biases, indicating that neither factor alone adequately explained the observed bias variations.

Overall, the A-EBD product provides useful observations for characterizing the main vertical structures of dust layers over the Taklamakan Desert. However, quantitative applications require quality screening and uncertainty assessment that account for differences among parameters, stations, and altitudes. In particular, interpretations of particle properties based on depolarization ratio and lidar ratio should be supported by independent observations.

Code and data availability

The EarthCARE/ATLID L2A A-EBD data used in this study are available from ESA's Multi-mission Algorithm and Analysis Platform (MAAP, https://portal.maap.eo.esa.int/). The analysis code and derived data supporting the findings of this study are openly available on Zenodo at https://doi.org/10.5281/zenodo.23720030.

Author contributions

Yabin Wei conducted the analysis and validation, created the visualizations, and wrote the original draft of the manuscript. Yu Wang and Ali Mamtimin designed the study and contributed key ideas as well as the review and revision of the manuscript. Jiacheng Gao and Meiqi Song provided the data. Meiqi Song, Yu Wang and Yabin Wei interpreted the data. Yakupujiang Abuduaini, Cong Wen and Qing Gong contributed to the interpretation and writing of the paper with contributions from the coauthors.

https://doi.org/10.5194/egusphere-2026-6659
Preprint. Discussion started: 22 November 2026
© Author(s) 2026. CC BY 4.0 License.

Competing interests

The authors declare that they have no conflict of interest.

Financial support

This research was funded by the Tianshan Talent Training Program–Youth Talent Support Project (2024TSYCQNTJ0002), the China Desert Meteorological Research Fund (Grant Sqj2025007), the First-Class Scientific and Technological Leadership Talent Project of the Xinjiang Strategic Talent Cultivation Program (XJRC-2025- KJ-PY-KJLJ-089), the CMA Meteorological Capacity Enhancement Joint Research Special Project (No. 24NLTSZ006), the S&T Development Fund of CAMS (CXFZ2026J142), The Xinjiang Key Laboratory of Desert Meteorology and Sandstorms Award Funding: Grant number: 2023-38 and Development Fund of CAMS (2021KJ034).

References

Ansmann, A., Wandinger, U., Riebesell, M., Weitkamp, C., and Michaelis, W.: Independent measurement of extinction and backscatter profiles in cirrus clouds by using a combined Raman elastic-backscatter lidar, Appl. Opt., 31, 7113–7131, 10.1364/AO.31.007113, 1992.

Baars, H., Haarig, M., König, L., Floutsi, A. A., Basharova, E., Hofer, J., Gebauer, H., Engelmann, R., Althausen, D., Skupin, A., Gast, B., Fritzsch, F., Ohneiser, K., Jimenez, C., Gaudek, T., Radenz, M., Buholdt, H., Heese, B., Klamt, A., Seifert, P., Donovan, D. P., van Zadelhoff, G. J., Abdullaev, S. F., Khalifaeva, S. K., Nozirov, D. F., and Wandinger, U.: Validation of EarthCARE/ATLID aerosol profiling products with ground-based PollyNET lidars – case studies, Atmos. Meas. Tech., 19, 3831–3864, 10.5194/amt-19-3831-2026, 2026.

Benavent-Oltra, J. A., Casquero-Vera, J. A., Román, R., Lyamani, H., Pérez-Ramírez, D., Granados-Muñoz, M. J., Herrera, M., Cazorla, A., Titos, G., Ortiz-Amezcua, P., Bedoya-Velásquez, A. E., de Arruda Moreira, G., Pérez, N., Alastuey, A., Dubovik, O., Guerrero-Rascado, J. L., Olmo-Reyes, F. J., and Alados-Arboledas, L.: Overview of the SLOPE I and II campaigns: aerosol properties retrieved with lidar and sun–sky photometer measurements, Atmos. Chem. Phys., 21, 9269–9287, 10.5194/acp-21-9269-2021, 2021.

Chen, Z., Zhou, C., Gao, J., Zhu, C., Song, M., Wang, Y., Wei, Y., Meng, L., Ma, M., and Wen, C.: Response of extreme precipitation to dust aerosols in the Tarim Basin over the past 50 years, Atmos. Chem. Phys., 26, 3853–3866, 10.5194/acp-26-3853-2026, 2026.

Donovan, D. P., van Zadelhoff, G. J., and Wang, P.: The EarthCARE lidar cloud and aerosol profile processor (A-PRO): the A-AER, A-EBD, A-TC, and A-ICE products, Atmos. Meas. Tech., 17, 5301–5340, 10.5194/amt-17-5301-2024, 2024.

https://doi.org/10.5194/egusphere-2026-6659
Preprint. Discussion started: 22 November 2026
© Author(s) 2026. CC BY 4.0 License.

Eisinger, M., Marnas, F., Wallace, K., Kubota, T., Tomiyama, N., Ohno, Y., Tanaka, T., Tomita, E., Wehr, T., and Bernaerts, D.: The EarthCARE mission: science data processing chain overview, Atmos. Meas. Tech., 17, 839–862, 10.5194/amt-17-839-2024, 2024.

Fernald, F. G.: Analysis of atmospheric lidar observations: some comments, Appl. Opt., 23, 652–653, 10.1364/AO.23.000652, 1984.

Floutsi, A. A., Rizos, K., Trapon, D., Engelmann, R., Althausen, D., Marinou, E., Paschou, P., Hofer, J., Proestakis, E., Gebauer, H., Skupin, A., Ansmann, A., Fehr, T., Hummel, T., Koopman, R., Amiridis, V., Wandinger, U., and Baars, H.: On the representativeness of the ground-based lidar observations for satellite calibration/validation – the example of the archipelago of Cabo Verde, Atmos. Meas. Tech., 19, 1901–1925, 10.5194/amt-19-1901-2026, 2026.

Freudenthaler, V.: About the effects of polarising optics on lidar signals and the Δ90 calibration, Atmos. Meas. Tech., 9, 4181–4255, 10.5194/amt-9-4181-2016, 2016.

Hong, Y. and Di Girolamo, L.: An Overview of Aerosol Properties in Clear and Cloudy Sky Based on CALIPSO Observations, Earth and Space Science, 9, e2022EA002287, https://doi.org/10.1029/2022EA002287, 2022.

Huang, J., Wang, T., Wang, W., Li, Z., and Yan, H.: Climate effects of dust aerosols over East Asian arid and semiarid regions, Journal of Geophysical Research: Atmospheres, 119, 11,398–311,416, https://doi.org/10.1002/2014JD021796, 2014.

Huang, J., Lin, B., Minnis, P., Wang, T., Wang, X., Hu, Y., Yi, Y., and Ayers, J. K.: Satellite-based assessment of possible dust aerosols semi-direct effect on cloud water path over East Asia, Geophysical Research Letters, 33, https://doi.org/10.1029/2006GL026561, 2006.

Jin, L., He, Q., Li, Z., Deng, M., and Abbas, A.: Variation characteristics of dust in the Taklimakan Desert, Natural Hazards, 120, 2129–2153, 10.1007/s11069-023-06269-3, 2024.

Kim, M. H., Omar, A. H., Tackett, J. L., Vaughan, M. A., Winker, D. M., Trepte, C. R., Hu, Y., Liu, Z., Poole, L. R., Pitts, M. C., Kar, J., and Magill, B. E.: The CALIPSO version 4 automated aerosol classification and lidar ratio selection algorithm, Atmos. Meas. Tech., 11, 6107–6135, 10.5194/amt-11-6107-2018, 2018.

Kok, J. F., Storelvmo, T., Karydis, V. A., Adebiyi, A. A., Mahowald, N. M., Evan, A. T., He, C., and Leung, D. M.: Mineral dust aerosol impacts on global climate and climate change, Nature Reviews Earth & Environment, 4, 71–86, 10.1038/s43017-022-00379-5, 2023.

Kylling, A., Vandenbussche, S., Capelle, V., Cuesta, J., Klüser, L., Lelli, L., Popp, T., Stebel, K., and Veefkind, P.: Comparison of dust-layer heights from active and passive satellite sensors, Atmos. Meas. Tech., 11, 2911–2936, 10.5194/amt-11-2911-2018, 2018.

Mamouri, R. E., Amiridis, V., Papayannis, A., Giannakaki, E., Tsaknakis, G., and Balis, D. S.: Validation of CALIPSO space-borne-derived attenuated backscatter coefficient profiles using a ground-based lidar in Athens, Greece, Atmos. Meas. Tech., 2, 513–522, 10.5194/amt-2-513-2009, 2009.

Omar, A. H., Winker, D. M., Vaughan, M. A., Hu, Y., Trepte, C. R., Ferrare, R. A., Lee, K.-P., Hostetler, C. A., Kittaka, C., Rogers, R. R., Kuehn, R. E., and Liu, Z.: The CALIPSO Automated Aerosol Classification and Lidar Ratio Selection

https://doi.org/10.5194/egusphere-2026-6659
Preprint. Discussion started: 22 November 2026
© Author(s) 2026. CC BY 4.0 License.

Algorithm, Journal of Atmospheric and Oceanic Technology, 26, 1994–2014, https://doi.org/10.1175/2009JTECHA1231.1, 2009.

Remer, L. A., Levy, R. C., and Martins, J. V.: Opinion: Aerosol remote sensing over the next 20 years, Atmos. Chem. Phys., 24, 2113–2127, 10.5194/acp-24-2113-2024, 2024.

Song, Q., Zhang, Z., Yu, H., Ginoux, P., and Shen, J.: Global dust optical depth climatology derived from CALIOP and MODIS aerosol retrievals on decadal timescales: regional and interannual variability, Atmos. Chem. Phys., 21, 13369–13395, 10.5194/acp-21-13369-2021, 2021.

van Zadelhoff, G. J., Donovan, D. P., and Wang, P.: Detection of aerosol and cloud features for the EarthCARE atmospheric lidar (ATLID): the ATLID FeatureMask (A-FM) product, Atmos. Meas. Tech., 16, 3631–3651, 10.5194/amt-16-3631-2023, 2023.

Wandinger, U., Floutsi, A. A., Baars, H., Haarig, M., Ansmann, A., Hünerbein, A., Docter, N., Donovan, D., van Zadelhoff, G. J., Mason, S., and Cole, J.: HETEAC – the Hybrid End-To-End Aerosol Classification model for EarthCARE, Atmos. Meas. Tech., 16, 2485–2510, 10.5194/amt-16-2485-2023, 2023.

Wehr, T., Kubota, T., Tzeremes, G., Wallace, K., Nakatsuka, H., Ohno, Y., Koopman, R., Rusli, S., Kikuchi, M., Eisinger, M., Tanaka, T., Taga, M., Deghaye, P., Tomita, E., and Bernaerts, D.: The EarthCARE mission – science and system overview, Atmos. Meas. Tech., 16, 3581–3608, 10.5194/amt-16-3581-2023, 2023.

Winker, D. M., Vaughan, M. A., Omar, A., Hu, Y., Powell, K. A., Liu, Z., Hunt, W. H., and Young, S. A.: Overview of the CALIPSO Mission and CALIOP Data Processing Algorithms, Journal of Atmospheric and Oceanic Technology, 26, 2310–2323, https://doi.org/10.1175/2009JTECHA1281.1, 2009.

Winker, D. M., Pelon, J., Coakley, J. A., Ackerman, S. A., Charlson, R. J., Colarco, P. R., Flamant, P., Fu, Q., Hoff, R. M., Kittaka, C., Kubar, T. L., Le Treut, H., McCormick, M. P., Mégie, G., Poole, L., Powell, K., Trepte, C., Vaughan, M. A., and Wielicki, B. A.: The CALIPSO Mission: A Global 3D View of Aerosols and Clouds, Bulletin of the American Meteorological Society, 91, 1211–1230, https://doi.org/10.1175/2010BAMS3009.1, 2010.

Xing, Y., Chen, Y., Yan, S., Cao, X., Zhou, Y., Zhang, X., Shi, T., Niu, X., Wu, D., Cui, J., Zhou, Y., Wang, X., and Pu, W.: Dust storms from the Taklamakan Desert significantly darken snow surface on surrounding mountains, Atmos. Chem. Phys., 24, 5199–5219, 10.5194/acp-24-5199-2024, 2024.

Young, S. A. and Vaughan, M. A.: The Retrieval of Profiles of Particulate Extinction from Cloud-Aerosol Lidar Infrared Pathfinder Satellite Observations (CALIPSO) Data: Algorithm Description, Journal of Atmospheric and Oceanic Technology, 26, 1105–1119, https://doi.org/10.1175/2008JTECHA1221.1, 2009.

Yumimoto, K., Eguchi, K., Uno, I., Takemura, T., Liu, Z., Shimizu, A., and Sugimoto, N.: An elevated large-scale dust veil from the Taklimakan Desert: Intercontinental transport and three-dimensional structure as captured by CALIPSO and regional and global models, Atmos. Chem. Phys., 9, 8545–8558, 10.5194/acp-9-8545-2009, 2009.

https://doi.org/10.5194/egusphere-2026-6659
Preprint. Discussion started: 22 November 2026
© Author(s) 2026. CC BY 4.0 License.



Zhou, C., Liu, Y., He, Q., Zhong, X., Zhu, Q., Yang, F., Huo, W., Mamtimin, A., Yang, X., Wang, Y., and Meng, L.: Dust Characteristics Observed by Unmanned Aerial Vehicle over the Taklimakan Desert, Remote Sensing, 14, 990, 10.3390/rs14040990, 2022.

Zhou, C., Liu, Y., Li, D., Zhu, Q., Tan, Z., Luo, R., Song, M., Zhu, C., Wang, Y., Mamtimin, A., Yang, X., Yang, F., Huo, W., Gao, J., Ma, M., and Wang, T.: Multisource Observations of Dust Rain in the Tarim Basin: Dust Events Act as a Trigger for Rainfall, ACS ES&T Air, 2, 2275–2287, 10.1021/acsestair.5c00217, 2025.